Journal of Hazardous Materials 384 (2020) 121447

Contents lists available at ScienceDirect

Journal of Hazardous Materials

journal homepage: www.elsevier.com/locate/jhazmat

Facilely synthesized cobalt doped hydroxyapatite as hydroxyl promoted peroxymonosulfate activator for degradation of Rhodamine B

Yixiong Pang[a,c], Lingjun Kong[a,b,d,*], Diyun Chen[a,*], Gutha Yuvaraja[a,c], Sajid Mehmood[a,c]

[a] Guangdong Provincial Key Laboratory of Radionuclides Pollution Control and Resources, School of Environmental Science and Engineering, Guangzhou University, Guangzhou, 510006, China

[b] Guangdong Key Laboratory of Environmental Catalysis and Health Risk Control, School of Environmental Science and Engineering, Institute of Environmental Health and Pollution Control, Guangdong University of Technology, Guangzhou, 510006, China

[c] School of Civil Engineering, Guangzhou University, Guangzhou, 510006, China

[d] Department of Civil Engineering, The University of Hong Kong, Pokfulam Road, Hong Kong, China

GRAPHICAL ABSTRACT

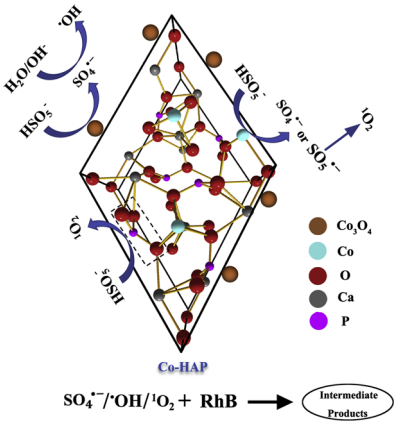

ARTICLE INFO

Editor: Xiaohong Guan

Keywords:
Co-hydroxyapatite
Cobalt-based catalyst
PMS
Co-catalytic
RhB

ABSTRACT

Hydroxyapatite (HAP) is a promising supporter of catalyst due to its potential in immobilizing metals stably. HAP supported cobalt-based catalyst (Co-HAP) was synthesized via a facile ion exchange-calcination method to reduce the Co leaching. The synthesized Co-HAP was characterized by X-ray diffraction (XRD), Scanning electron microscopy (SEM), Transmission electron microscope (TEM), Brunauer-Emmett-Teller (BET) analysis and X-ray photoelectron spectroscopy (XPS). Cobalt ions were incorporated into HAP structure and Co_3O_4 on HAP surface. Co-HAP showed satisfactory performance in peroxymonosulfate (PMS) activation for eliminating Rhodamine B (RhB) in aqueous solution. Co-HAP even revealed a better activity than that of $CoFe_2O_4$. •OH, $SO_4^{\bullet-}$ and $^1O_2$ were all involved in RhB degradation and $^1O_2$ played a leading role. High content of surface oxygen groups could be found on Co-HAP after RhB degradation, which might be resulted from the high amounts of hydroxyl groups. The presence of hydroxyl groups performed the co-catalytic activity of PMS activation in Co-HAP/PMS system.

* Corresponding authors at: Guangdong Provincial Key Laboratory of Radionuclides Pollution Control and Resources, School of Environmental Science and Engineering, Guangzhou University, Guangzhou, 510006, China.

E-mail addresses: kongl_jun@163.com (L. Kong), cdy@gzhu.edu.cn (D. Chen).

https://doi.org/10.1016/j.jhazmat.2019.121447
Received 10 June 2019; Received in revised form 6 October 2019; Accepted 9 October 2019
Available online 09 October 2019
0304-3894/

1. Introduction

Nowadays, sulfate radical-based advanced oxidation processes have gained considerable attention in the treatment of refractory organic wastewater. Moreover, sulfate radical oxidation is regarded to be more promising than hydroxyl radical oxidation owing to its high redox potential of 1.8–2.7 V NHE, wide applicable scope of pH and long lifetime of 30–40 μS (Huang et al., 2017). The $SO_4^{\bullet-}$ can be generated from the decomposition of peroxymonosulfate (PMS) though energy-based activation (e.g., microwave (Qi et al., 2017), UV (Guan et al., 2018) or ultrasound (Yin et al., 2018)) and catalytic activation with metal-free catalysts (e.g., nitrogen-doped graphene (Wang et al., 2017), nitrogen-functionalized sludge carbon (Sun et al., 2017)) or transition metals (e.g., Co_3O_4 (Yuan et al., 2018), ferrite (Guan et al., 2013), Fe_3O_4/β-FeOOH (Li et al., 2019a), Co_3S_4@GN (Zhu et al., 2019), CoMgAl oxides (Hong et al., 2019)). Among them, the activation via catalyst is regarded as an acceptable method for industrial application owing to the fact of free external energy input in the reaction. Based on the results in previous reports, cobalt based materials were considered to be more efficient than other transition metal catalysts in PMS activation (Hu and Long, 2016). However, the Co-based activated PMS process has the risk of toxic transition metal leaching, which limits its further application. Hence, numerous studies are engaged in overcoming the drawback of transition metal activation. In general, there are two ways for reducing cobalt ion leaching. One is synthesizing more stable combined transition metal oxides, such as Co_3O_4-Bi_2O_3 (Hu et al., 2018a), $CoFe_2O_4$ (Yang et al., 2018b), Co_3O_4-TiO_2 (Zhang et al., 2018), the other is combining transition metal with supporter to provide high activity catalyst, such as Co-zeolite (Cong et al., 2017), Co_3O_4-AC (Xie et al., 2018b), Co_3O_4-biochar (Chen et al., 2018).

Recently, hydroxyapatite (HAP, $Ca_{10}(PO_4)_6(OH)_2$), an important component of biological skeleton, has been widely used in environmental remediation owing to its excellent biocompatibility, stability and high specific surface area. HAP is generally employed to adsorb heavy metal in aqueous solution, due to its ability of cation exchanging (Han et al., 2018; Hao et al., 2017; Wang et al., 2018). In these cases, the heavy metals can be immobilized on the HAP stably. HAP has a similar character as zeolite (Šljivić Ivanović et al., 2013), what could be considered as a supporter of catalyst. Thus, more attentions were paid on the metal-hydroxyapatite as green and stable catalysts in heterogeneous photocatalytic reaction (Hu et al., 2018b) and Fenton-like degradation (Valizadeh et al., 2014). For example, as reported by Liu et al. (2014), Fe-HAP was synthesized facilely by a ion-exchange method and revealed promising visible-light photocatalytic activity toward organic dye degradation. Fortunately, PMS activation by the hydroxyapatite recovered Co^{2+} was reported (Song et al., 2018), which provided a new insight into understanding the application of metal-hydroxyapatite in PMS activation. Formation of Co^{2+} with H_2O into $CoOH^+$ contributed to PMS activation. This new finding encourages us to investigate the synthesis of Co-hydroxyapatite for PMS activation, in

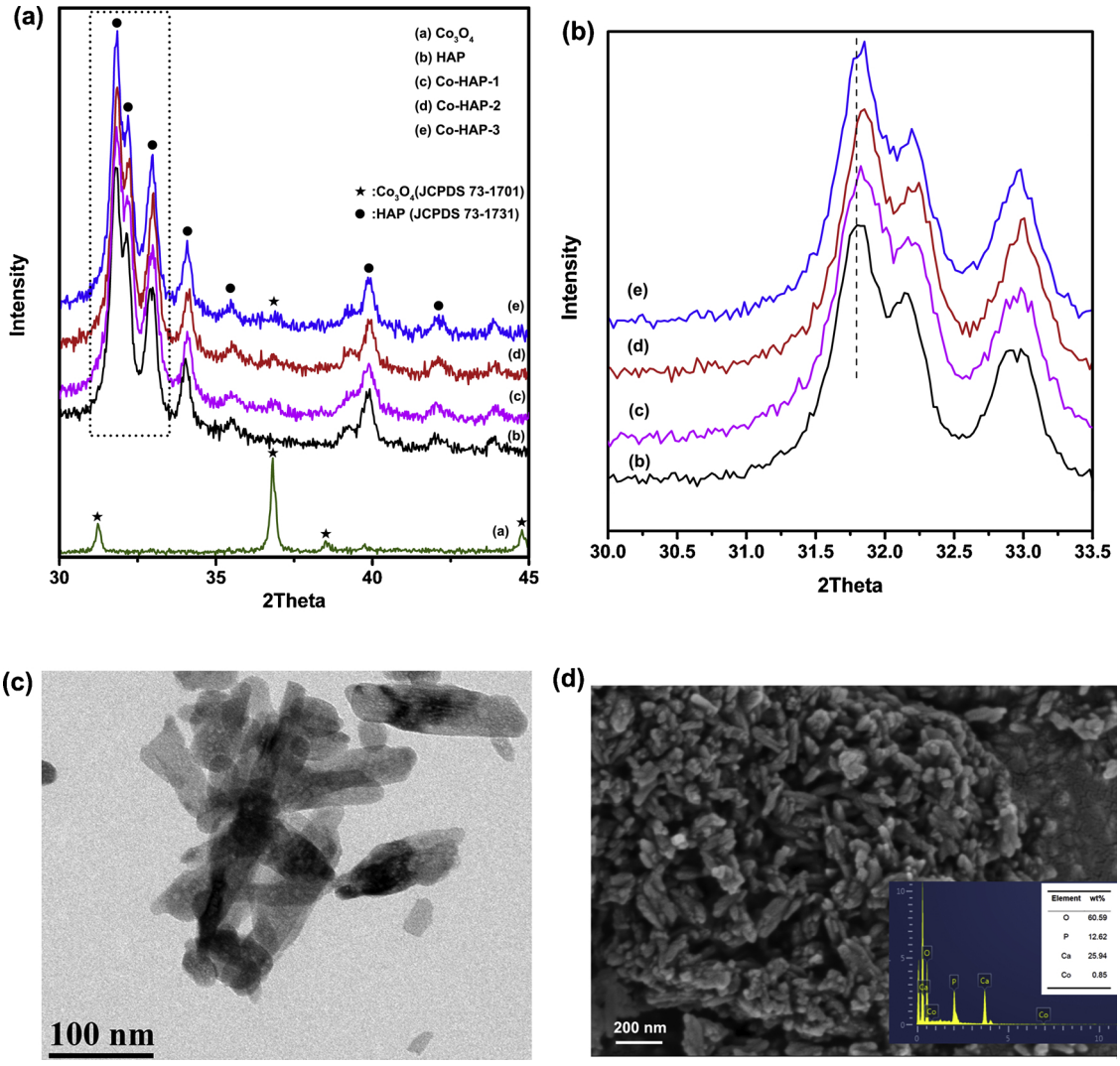

Fig. 1. XRD spectra (a and b) of synthesized samples. TEM (c) and SEM (Inset: EDS results) (d) images of Co-HAP-2.

which the Co element could be immobilized on hydroxyapatite to address the issue of cobalt ion leaching.

In this work, Co-HAP as a PMS activator for organic contaminants degradation was facilely synthesized via a two steps method (ion exchange and calcination), in which the HAP was a supporter for immobilizing Co. More excitingly, the HAP is hypothesized to be a promoter for activating PMS since the HAP is rich in hydroxyl group. The synthesized Co-hydroxyapatites were characterized by XRD, SEM, TEM, BET analysis and XPS. The mechanism of the Co-HAP for PMS activation was investigated by quenching experiments and EPR analysis. Especially the promoted catalytic effect of hydroxyl group on PMS activation for RhB degradation was understood via ATR-FTIR and XPS analysis. The pathway of RhB degradation in the Co-HAP activated PMS process was also understood.

2. Material and methods

2.1. Materials and chemicals

The details were given in Supplementary Information.

2.2. Preparation of catalysts

Co-HAP sample was synthesized using a modified method described by previous report (Liu et al., 2014). A certain amount of cobalt (II) nitrate was dissolved into 100 mL pure water. Then 1.0 g of HAP was added into this solution and vigorously magnetic stirred at ambient temperature for 15 min. Cobalt (II) was exchanged into HAP by mixing it with the cobalt (II) nitrate solutions in 10, 25 and 50 mmol/L, respectively. The generated pink precipitates were washed for several times and collected by filtration. The precursors were dried in the oven at 80 °C for 12 h and calcinated at 500 °C for 4 h in the air atmosphere. The samples, which exchanged with cobalt (II) of 10, 25 and 50 mmol/L, were denoted as Co-HAP-1, Co-HAP-2 and Co-HAP-3, respectively. In order to compare the catalytic performance of Co-HAP with other catalysts, Co_3O_4 was synthesized by direct pyrolysis of $Co(NO_3)_2$ at 500 °C for 4 h and $CoFe_2O_4$ was prepared via a solvothermal method described in previous reports. (Shen et al., 2015).

2.3. Characterization

The details were given in Supplementary Information.

2.4. Degradation of RhB

Typically, in each experiment, 100 mL of 40 mg/L RhB aqueous solution was mixed with 20 mg catalyst. The initial pH value of RhB solution is 5.5 without adjustment. 0.4 mL of PMS solution (0.1 mol/L) was added to the suspension. At given time intervals, 5 mL of sample was immediately blended with the same volume of pure methanol to terminate the reaction. Quenching experiments were carried out by using methanol, tert-butyl alcohol (TBA) and L-Histidine. The designated concentration of quencher was added into the solution before the adding of PMS. Degradation of LFX, AO7 and TCH were conducted by the same process as RhB degradation. The residual concentration of RhB, LFX, AO7 and TCH was measured by UV–vis spectrophotometry at 554, 286, 484 and 360 nm wavelength, respectively. Total organic carbon concentration was determined via Shimadzu TOC analyzer (TOC-L). The degradation intermediates were identified by UPLC-MS-MS (Waters Xevo TQ-S Micro) with a C18 column (2.1 × 50 mm) and the details were given in Supplementary Information.

3. Results and discussion

3.1. Characterization of Co-HAP

The crystalline structures of bulk HAP, synthesized Co_3O_4 and Co-HAP samples were characterized by XRD. As displayed in Fig. 1a, the peaks which denoted as circle were well matched with the crystal planes of hydroxyapatite (JCPDS No. 73-1731). No obvious change occurred on these peaks of Co-HAP samples, suggesting that the crystalline nature of HAP is stable even after calcination. Obviously, Co_3O_4 (JCPDS No. 73-1701) could be obtained from direct calcination of $Co(NO_3)_2$, implying that Co_3O_4 may form on HAP with a similar synthesis method. The XRD patterns of Co-HAP samples calcined at 500 °C revealed a new tiny diffraction peaks (denoted as star) at 2Theta value of 36.85° which could be ascribed to (3 1 1) crystal plane of Co_3O_4 (JCPDS No. 73-1701), evidencing that the partial Co species existed on Co-HAP sample in the form of Co_3O_4. Furthermore, as shown in Fig. 1b, the peaks of HAP shifted to a little higher 2Theta angle after Co loading, suggesting that there had been an lattice distortion in HAP structure (Jung et al., 2019). This was ascribed to the exchange of Ca^{2+} ions (0.100 nm) with smaller Co^{2+} ions (0.074 nm) in the lattice structure of hydroxyapatite. Hence, the XRD result confirmed that Co species existed on HAP in form of Co_3O_4 on HAP surface and lattice Co (Co_{lat}) in HAP crystal. The actual Co loading amounts were determined by ICP-MS, which were 1.3%, 2.0% and 2.2% for Co-HAP-1, Co-HAP-2 and Co-HAP-3, respectively.

The TEM, SEM images and EDS spectrum of Co-HAP-2 are shown in Fig. 1c and d, respectively. The size of the cobalt doped HAP samples was about 150 nm in length. The element composition of the Co-HAP was confirmed by the presence of P, O, H, Ca and Co elements from EDS analysis (Fig. 1d inset). The weight content of Co element was evaluated to 0.85%, evidencing the loading of Co elements in the Co-HAP. The surface chemical composition of Co-HAP was investigated by XPS. The XPS survey spectra of HAP, Co-HAP-2 before and after reaction are shown in Fig. 5a. The XPS survey spectrum of HAP shows the characteristic peaks of P, Ca and O, which are typical chemical elements from HAP. Moreover, For Co-HAP-2, a new peak was found at between 781.8 to 810 eV, which attributed to Co 2p, indicating that Co species exists on Co-HAP-2 surface. After the RhB degradation, no peak disappeared in used Co-HAP-2 spectra, indicating that the surface chemical composition of Co-HAP-2 was stable during the PMS activation. The BET surface areas of synthesized materials are shown in Table 1. Obviously, Co-HAP samples have much larger specific surface areas of 45.05 to 52.68 m^2/g than that of Co_3O_4 (1.82 m^2/g). It is expected that higher activity can be observed because BET surface area usually shows a positive correlation with active sites (Chen et al., 2018).

3.2. Catalytic performance

The catalytic activity of synthesized samples was evaluated by degradation of RhB via PMS activation. The UV–vis absorbance spectra changes of RhB solutions during the degradation in Co-HAP-2/PMS process are shown in Fig. 2a. The typical absorption peak of RhB located at 554 nm remarkably decreased to about 60% within 2 min. This result suggests that conjugated xanthene structure could be destructed during RhB degradation (Hu et al., 2017). Fig. 2b shows the

Table 1
BET surface area of different samples.

Sample	BET surface area (m^2/g)
Co_3O_4	1.82
HAP	73.87
Co-HAP-1	52.68
Co-HAP-2	51.09
Co-HAP-3	46.84

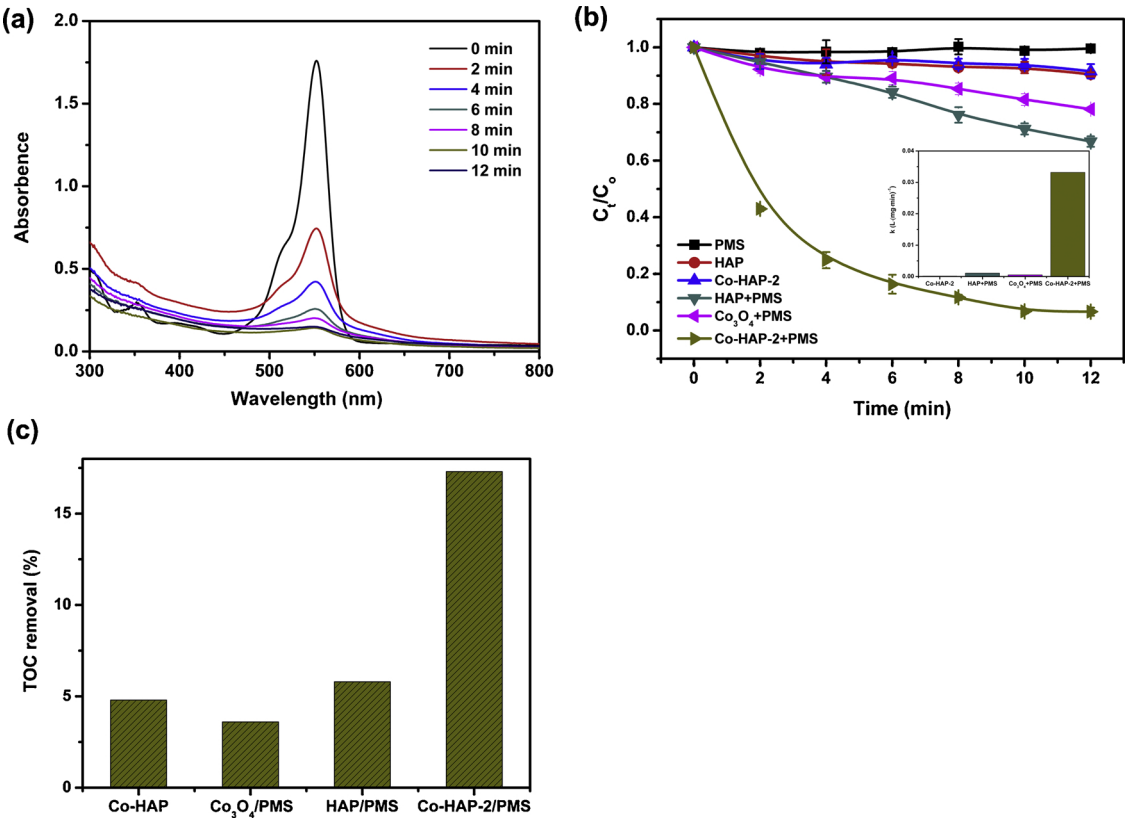

Fig. 2. The UV–vis absorbance spectra of RhB solution with different reaction time (a) and degradation of RhB in different systems (b). (c) TOC removal in different systems. Reaction conditions: initial [RhB] = 40 mg/ L, initial pH = 5.5, [PMS] = 0.4 mmol/L and [Catalyst] = 0.2 g/L.

degradation dynamic curves of RhB varying with reaction time over HAP, Co_3O_4 and synthesized Co-HAP-2. It could be found that only about 10% of RhB was removed over HAP or Co-HAP-2 without addition of PMS, which was ascribed to adsorption, suggesting that adsorption made a negligible contribution to RhB degradation. The degradation efficiency of RhB was only about 23% due to Co_3O_4 activated PMS process which was widely reported. Interestingly, 33.4% of RhB was degraded in HAP/PMS system, suggesting that HAP performed the ability of PMS activation. Since the HAP is composed of calcium phosphate and hydroxyl, the PMS activation may be ascribed to the chemical group of HAP. It was clearly discussed in section 3.3. Surprisingly, the degradation efficiency of RhB increased significantly once cobalt was loaded on HAP. The degradation efficiency of RhB reached 93.3% within 12 min in the presence of Co-HAP-2. The result was greater than the sum of the degradation efficiencies of RhB in the presence of Co_3O_4 and HAP activated PMS. Additionally, the pseudo second-order kinetic model could fit well to the RhB degradation efficiencies as a function of reaction time. The obtained reaction rate constant of Co-HAP is 0.0332 L•(mg min)$^{-1}$, which is much higher than the sum of those of Co_3O_4 and HAP, suggesting that the combination of cobalt species and HAP had synergistic effect on PMS activation. Furthermore, as can be seen in Fig. 2c, after reaction time of 12 min, TOC removal of 17.5% could be achieved in Co-HAP-2/PMS system. Although Co-HAP-2 showed high activity, Co loaded catalysts for PMS activation were common. Hence, the comparison between Co-HAP and other cobalt loaded catalysts is given in Table 2. Obviously, some catalysts may display higher activities than that of Co-HAP. However, the synthesis of these catalysts needed complicate methods or expensive material (e.g. GO and RGO), which limited their industrial application. Facilely synthesized Co-HAP may be more suitable for large-scale production than those catalysts.

The influences of PMS concentration and Co-HAP-2 dosage on RhB degradation were presented in Fig. 3a and b. Obviously, the degradation process was positive dependence on PMS dosage. In the presence of Co-HAP-2, RhB degradation efficiency increased from 79.0% to 93.3% with the PMS concentration increased from 0.2 to 0.4 mmol/L, respectively. It can be inferred that more reactive oxygen species (ROS) were generated through PMS decomposition as more PMS was added. Although the increasing in PMS dosage was beneficial for RhB degradation, excessive PMS dosage led to a slight reduction in RhB degradation which might be attributed to the self-quenching effect between HSO_5^- and ROS (Liu et al., 2019). Additionally, pseudo first and second-order kinetic models were used to fit the RhB degradation data with deferent PMS dosages. As shown in Table 3, higher correlation

Table 2
Comparison of different catalysts for PMS activation.

Catalyst	Organic pollutant	Initial concentration	Reaction time (min)	Degradation efficiency
Co_3O_4/NF (Yuan et al., 2018)	Acid Orange 7	0.1 mmol/L	30	~100%
RGO/Fe_3O_4–Co_3O_4 (Zhang et al., 2017)	Orange II	0.2 mmol/L	5	~100%
Co_3O_4-biochar (Chen et al., 2018)	Ofloxacin	50 μmol/L	10	~90%
Hollow Co_3O_4/C (Abdul Nasir Khan et al., 2019)	Bisphenol A	87.6 μmol/L	4	97%
Co_3O_4/GO (Shi et al., 2014)	Acid Orange 7	0.6 mmol/L	4	~100%
Co-HAP (this work)	RhB	40 mg/L (0.083 mmol/L)	12	93.3%

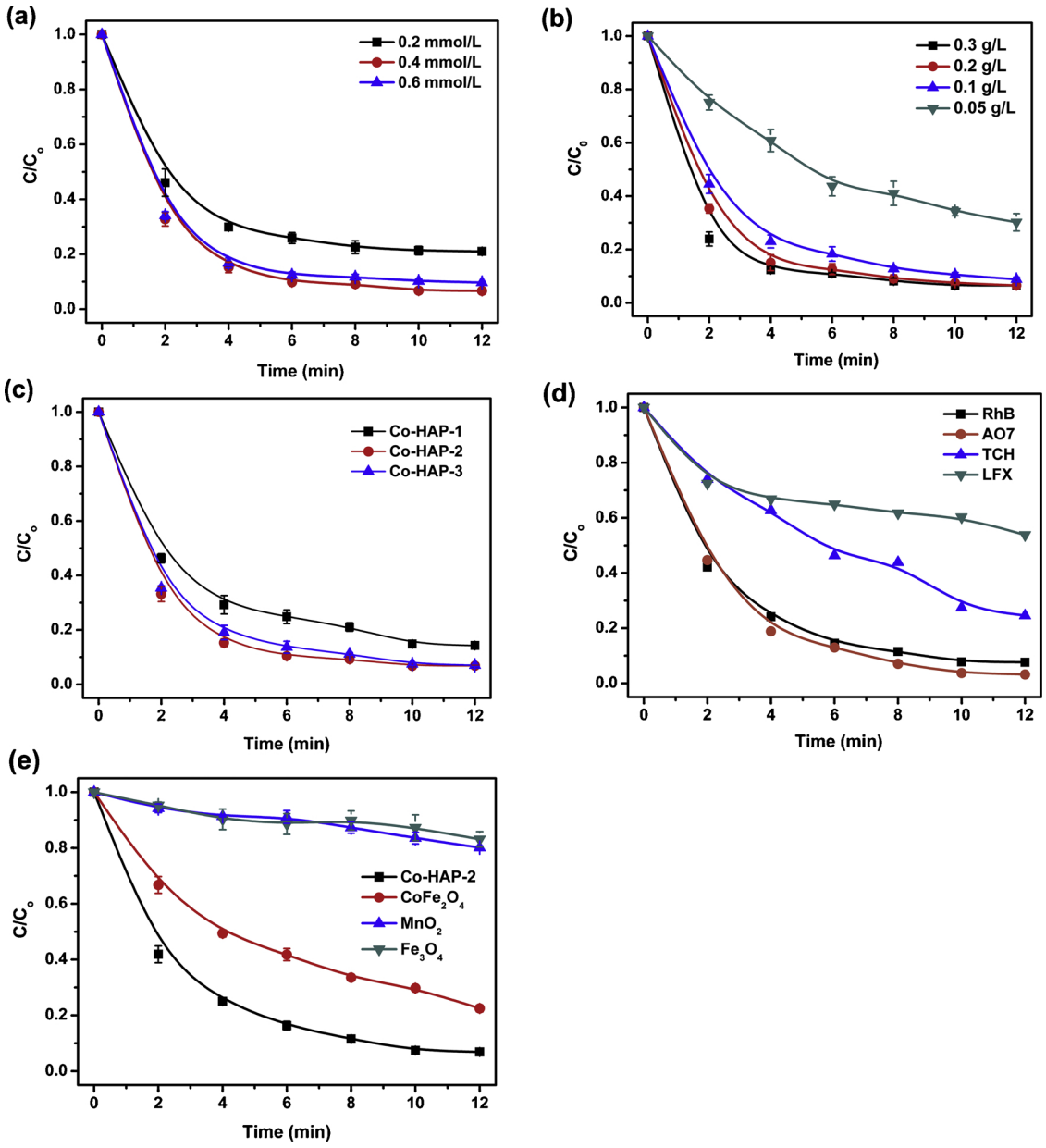

Fig. 3. The influence of (a) different PMS dosage, (b) different Co-HAP-2 dosage and (c) different Co loading on RhB degradation. (d) Degradation of different organic pollutants in Co-HAP-2/PMS system. (e) RhB degradation by PMS activation with common catalysts. Reaction conditions: unless otherwise specified, initial [RhB] = 40 mg/L, initial pH = 5.5, [PMS] = 0.4 mmol/L and [Catalyst] = 0.2 g/L.

coefficient could be obtained in pseudo second-order kinetic fitting, indicating that the degradation kinetics of RhB followed pseudo second-order kinetics. The rate constant reached maximum value of 0.0370 L•(mg• min)$^{-1}$ as the PMS dosage was 0.4 mmol/L. Generally, the degradation kinetics of organic contaminants in PMS-based process followed pseudo first-order kinetic model (Ding et al., 2019b; Li et al., 2019a; Lin et al., 2019). However, some researchers have found that the molar ratio of [PMS]/[Organic] caused the change of kinetic order (Ling et al., 2010; Yang et al., 2018a). The organic degradation followed the pseudo second-order model under the condition of lower [PMS]/[Organic] ratio. In this study, the molar ratio of [PMS]/[RhB] was ranged from 2.4 to 7.2, which might result in the change of kinetic order of RhB degradation.

There was a positive correlation between RhB degradation efficiencies and catalyst dosage when Co-HAP-2 dosage was increased from 0.05 to 0.2 g/L. In this case, the degradation efficiency of RhB increased from 69.8% to 93.5%, and the reaction constant increased from 0.0050 to 0.0328 L•(mg• min)$^{-1}$. The enhancement of RhB degradation was due to that more active site was provided as more catalyst was added. However, no significant further enhancement could be observed when the catalyst dosage was above 0.2 g/L, which might be resulted from the scavenging of generated •OH and $SO_4^{\bullet-}$ by excess Co(II) (Eq. 1 and Eq. 2) (Ding et al., 2019a).

$$SO_4^{\bullet-} + Co(II) \rightarrow SO_4^{2-} + Co(III) \quad (1)$$

$$\bullet OH + Co(II) \rightarrow OH^- + Co(III) \quad (2)$$

In the present work, obviously, the loaded Co species was the active site of Co-HAP catalyst. Therefore, the effect of Co loading on catalytic performance was also investigated by changing Co impregnation concentrations (0.01, 0.025 and 0.05 mol/L). As shown in Fig. 3c and Table 3, only 85.1% of RhB degradation efficiency and 0.0138 L•(mg• min)$^{-1}$ of reaction rate constant could be obtained in the presence of Co-HAP-1. Nevertheless, 93.0% of RhB could be eliminated within

Table 3
Pseudo first and second-order kinetic fitting for RhB degradation with different factors.

Factors	K_1 (min^{-1})	R_1^2	K_2 (L•(mg•min)$^{-1}$)	R_2^2
PMS dosage (mmol/L)				
0.2	0.143	0.7843	0.0096	0.9257
0.4	0.253	0.8496	0.0370	0.9901
0.6	0.213	0.7797	0.0233	0.9367
Catalyst dosage (g/L)				
0.05	0.107	09639	0.0050	0.9794
0.1	0.218	0.9153	0.0225	0.9902
0.2	0.247	0.8595	0.0328	0.9875
0.3	0.244	0.7878	0.0365	0.9827
Co impregnation concentrations (mol/L)				
0.01	0.172	0.8937	0.0138	0.9654
0.025	0.252	0.8568	0.0353	0.9837
0.05	0.239	0.8982	0.0305	0.9697

12 min for Co-HAP-2, and the reaction rate constant (0.0353 L•(mg• min)$^{-1}$) is about 2.5 times higher than that of Co-HAP-1. However, the further increasing in Co loading led to a slight decrease of degradation rate. In previous reports, excessive loading sometimes resulted in the inhabitation of catalyst activity (Ding et al., 2019b; Pi et al., 2020). For this work, excessive Co loading led to the agglomeration of catalyst particles, resulting in the reduction of active sites, which evidenced by BET results (Co-HAP-2: 51.09 m^2/g; Co-HAP-3: 46.84 m^2/g). Thus, the number of active sites might not increase as expected.

Several typical organic pollutants, such as Orange acid 7 (AO7), Tetracycline hydrochloride (TCH) and Levofloxacin (LFX), were also selected to estimate decontamination ability of Co-HAP/PMS system. As can be seen in Fig. 3d, Co-HAP-2/PMS showed different degradation performances toward these organic pollutants. LFX degradation efficiency only reached 46.2%, but 97.8% of AO7 degradation could be obtained with similar experiment conditions. The degradation efficiencies of organics followed the order: AO7 > RhB > TCH > LFX.

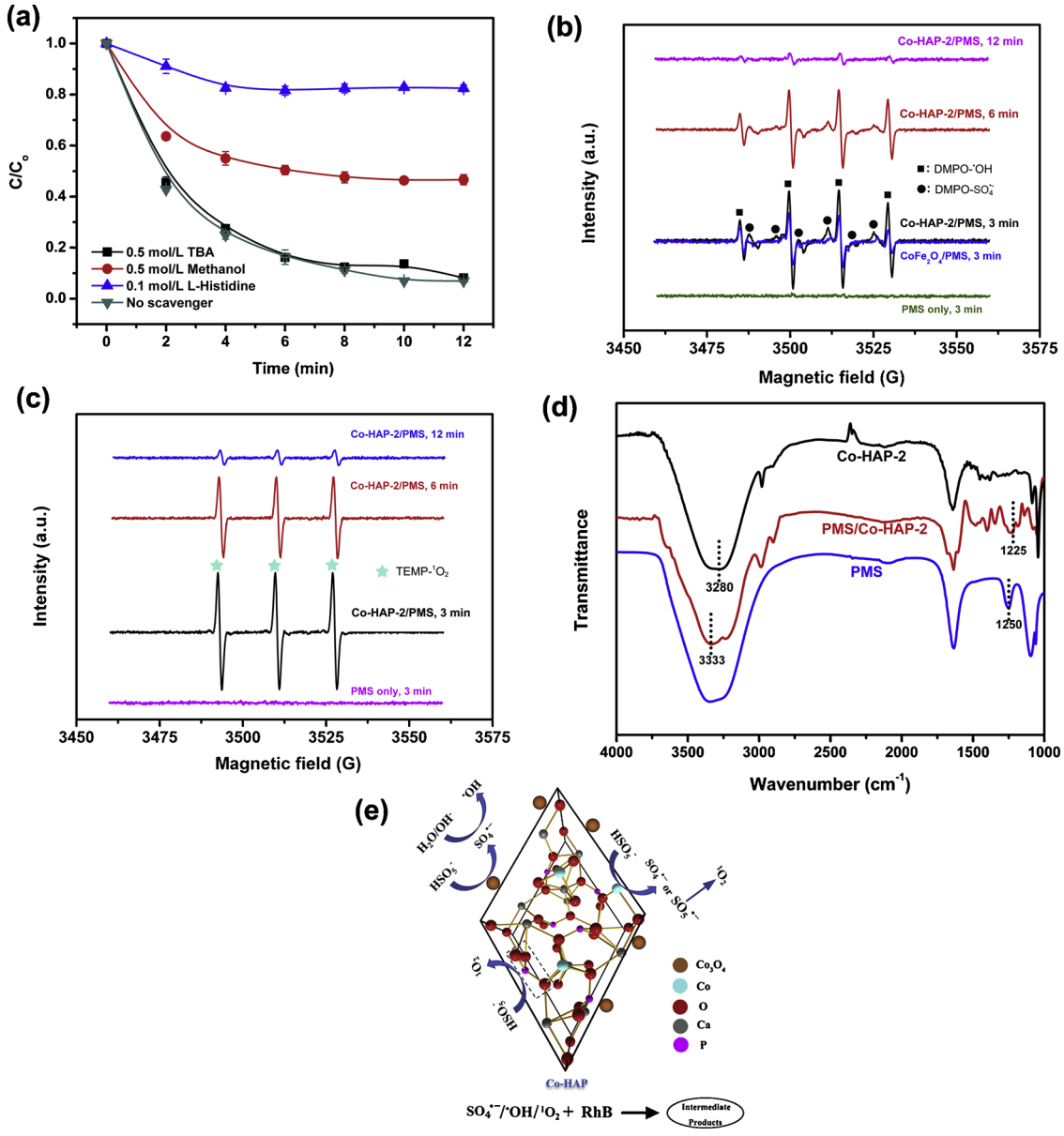

Fig. 4. (a) Influence of different scavengers on RhB degradation in Co-HAP-2/PMS system. Reaction conditions: initial [RhB] = 40 mg/ L, initial pH = 5.5, [PMS] = 0.4 mmol/L and [Catalyst] = 0.2 g/L. EPR spectra of (b) DMPO and (c) TEMP in PMS activation via Co-HAP-2 catalyst. (d) ATR-FTIR spectra of Co-HAP-2 in water, Co-HAP-2/PMS and PMS only systems. (e) The possible mechanism of ROS generation in Co-HAP-2/PMS system.

The difference in removal efficiencies of selected organic pollutants may be attributed to their different reactivity with sulfate radicals. It was found that the organic contaminants with electron donating groups can more easily reacted with $SO_4^{\bullet-}$ than those with electron withdrawing groups (Ding et al., 2019c). RhB and AO7 contain methyl and hydroxyl groups, respectively. These two groups both are electron donating groups, while TCH and LFX have -C(=O)N- and carboxyl groups, respectively, which both belong to electron withdrawing groups (Ye et al., 2017; Zhang et al., 2012). It might be the reason for the different removal efficiencies of these organic contaminants in Co-HAP/PMS system. In sum, it could be inferred that Co-HAP/PMS system has potential in oxidizing various type of organic pollutants.

The catalytic activities of three popular PMS activators ($CoFe_2O_4$ (Lin et al., 2018; Yang et al., 2018b), MnO_2 (Deng et al., 2017; Xie et al., 2018a) and Fe_3O_4 (Li et al., 2019a; Tan et al., 2014)) were also investigated for understanding the favorable catalytic activity of Co-HAP. Experimental results for RhB degradation with different heterogeneous catalysts are illustrated in Fig. 3e. Comparing with 92.1% degradation efficiency of RhB within 12 min achieved on Co-HAP-2, the degradation efficiencies of RhB were only 77.5%, 19.8%, and 16.9% for $CoFe_2O_4$, MnO_2, and Fe_3O_4, respectively. The RhB degradation efficiencies of different catalysts decreased as follows: Co-HAP-2 > $CoFe_2O_4$ > MnO_2 > Fe_3O_4, implying that Co-HAP-2 has highest catalytic activity, even better than $CoFe_2O_4$. The results obviously confirmed that the presence of HAP performed synergetic effect on PMS activation by Co species. Although metal-hydroxyapatites were widely reported in photocatalytic and Fenton catalytic processes, the synergetic effect of HAP during the catalytic process was freely reported. Since the hydroxyl group was widely reported during its cocatalytic effect on PMS activation (Chen et al., 2018; Zhang et al., 2018) and also the cocatalytic effect of hydroxyl group on SiO_2 was reported in our previous study (Tu et al., 2012), it is not hard to understand that surface hydroxyl group on the HAP played synergetic effect on Co-HAP activation of PMS. The HAP could be considered as a catalytic promoter, which played an important co-catalytic role in promoting the degradation of RhB in the PMS activation process.

3.3. Reaction mechanism and degradation pathway

3.3.1. Generation of reactive oxygen species

Quenching experiments were conducted to identify the generated ROS in RhB degradation. In these experiments, methanol and tert-butyl alcohol (TBA) were used as scavengers owing to their different reaction rate with hydroxyl and sulfate radicals. In general, the reaction rate between methanol and •OH ($k_{\bullet OH}$ = (3.8–7.6) × 10^8 M^{-1} s^{-1}) is almost 1000 times higher than that between TBA and $SO_4^{\bullet-}$ ($k_{SO4}^{\bullet-}$ = (4–9.1) × 10^5 M^{-1} s^{-1}) while the both methanol and TBA can react with $OH^{\bullet}$ rapidly (Yang et al., 2018c). Therefore, the roles of different free radicals could be evaluated according to the result of inhabitation effect of RhB degradation. As known to all, $^1O_2$ has been found in some PMS activation reactions (Li et al., 2019b; Zou et al., 2019). It could oxide organic contaminants via non-radical reaction. In this work, L-Histidine, a well-known $^1O_2$ quencher (Fu et al., 2019; Sun et al., 2019a), was employed to evaluate the contribution of non-radical reaction for RhB degradation. As shown in Fig. 4a, RhB degradation efficiency significantly decreased from 93% to 53% after the adding of 0.5 mol/L methanol. Conversely, TBA showed negligible inhibition in RhB degradation efficiency. It could be speculated that $SO_4^{\bullet-}$ was the main free radicals in RhB removal, which was generated in Co-HAP-2/PMS system. However, RhB degradation only reached 18% with the adding of L-histidine, suggesting that $^1O_2$ played a leading role in RhB degradation. To further understand the mechanism, EPR test was performed to identify the ROS generated in Co-HAP-2/PMS process. DMPO and TEMP were employed as spin trap agents in EPR test. The other detail conditions of EPR test were given in Text S3. As can be seen in Fig. 4b, no peak was found in EPR spectra of pure PMS because PMS

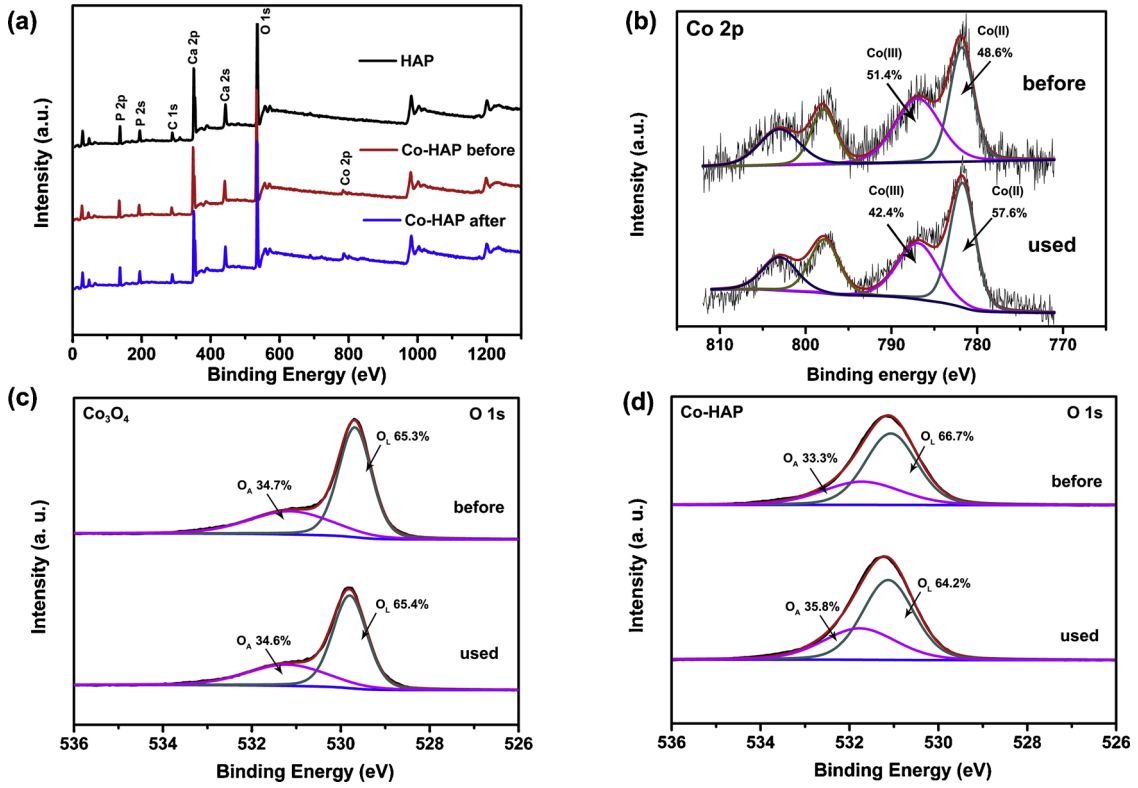

Fig. 5. XPS survey (a) and XPS spectra of (b) Co element in Co-HAP-2 before and after the reaction, O element in Co_3O_4 (c) and Co-HAP-2 (d) before and after the reaction.

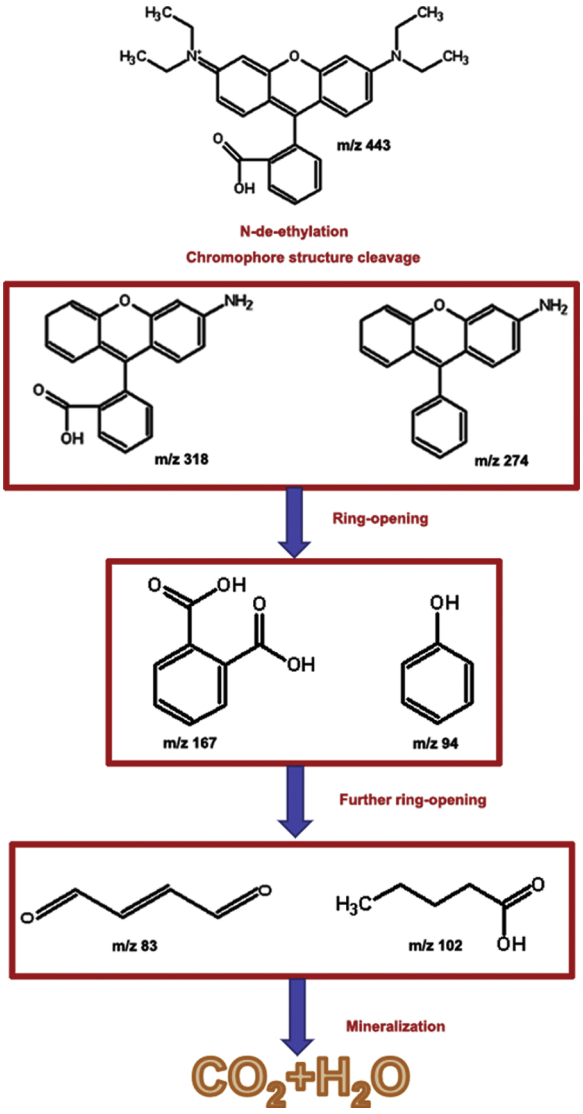

Fig. 6. The possible pathway of RhB degradation in Co-HAP-2/PMS system.

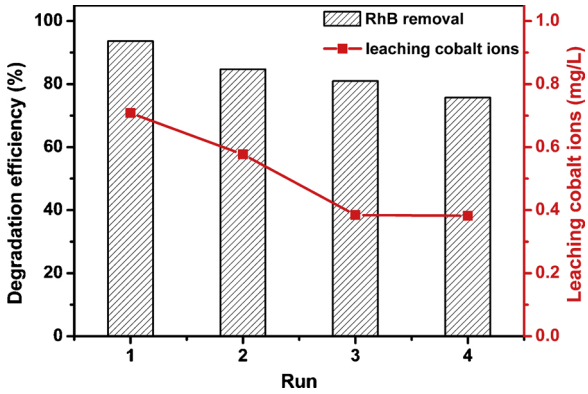

Fig. 7. RhB degradation and cobalt leaching in different reaction runs. Reaction conditions: initial [RhB] = 40 mg/ L, initial pH = 5.5, [PMS] = 0.4 mmol/L and $[Catalyst]_0$ = 0.3 g/L.

could not be activated without catalyst. Both DMPO- $SO_4^{\bullet-}$ and DMPO-•OH signals could be found during the reaction in the presence of Co-HAP-2 catalyst, suggesting that both two free radicals were generated in this system. It worth noting that the signals strength of DMPO- $SO_4^{\bullet-}$ and DMPO- •OH in Co-HAP-2/PMS system were higher than those in $CoFe_2O_4$/PMS system, implying that more free radicals were yielded in the Co-HAP-2/PMS system than those in $CoFe_2O_4$/PMS system. This could be resulted from the better catalytic effect on PMS activation of Co-HAP-2 than $CoFe_2O_4$. Additionally, as shown in Fig. 4c, no significant signal was detected for pure PMS. However, in the presence of Co-HAP-2, typical triplet peaks, which assigned to the TEMP-$^1O_2$, appeared in EPR spectra, confirming the generation of $^1O_2$ in the system. Briefly speaking, it could be speculated that both radical and non-radical reaction were involved in Co-HAP-2/PMS system and the $^1O_2$ was mainly responsible for RhB degradation.

FT-IR measurements can provide information of chemical bond between surface OH groups and PMS/PS (Lin et al., 2019; Wang et al., 2019b). In order to get insight into the catalytic mechanism of Co-HAP-2/PMS system, ATR-FTIR was applied to investigate the change of surface functional groups when Co-HAP-2 combined with PMS. As presented in Fig. 4d, the adsorption band at around 1250 cm^{-1} was attributed to the stretching of the S—O bonds of HSO_5^- (Shao et al., 2017). After the adding of Co-HAP-2, the band of 1250 cm^{-1} red-shifted 25 cm^{-1}, which might be resulted from Co(II)-(HO)OSO_3 complex (Wang et al., 2019a). The adsorption band located at 3281 cm^{-1} was assigned to the O—H stretching vibration. Moreover, this adsorption band shifted to 3333 cm^{-1} when the Co-HAP-2 was with PMS solution, suggesting that the HSO_5^- were combined with Co-HAP-2 with replacing some hydroxyl groups on the surface (Liu et al., 2015). These results indicate that surface hydroxyl groups on Co-HAP-2 participated in PMS activation.

Co species in PMS activation was investigated by XPS analysis to understand the catalytic effect on the generation of $SO_4^{\bullet-}$ and •OH in the Co-HAP/PMS system. As shown in Fig. 5b, two peaks located at 781.8 and 786.9 eV were attributed to Co(II) and Co(III). The relative proportion to the total Co species were 48.6% and 51.4% for Co(II) and Co (III) before the reaction, respectively. However, the relative proportion of Co(II) increased to 57.6% after the reaction, indicating that Co ion participated in PMS activation though Co-HAP catalyst. These results imply that a redox cycle of the Co species (Co^{2+}→Co^{3+}→Co^{2+}) could occur during PMS activation. Based on the above results and previous reports, the generation of free radicals in Co-HAP/PMS system would follow these steps: (1) The Co_{lat} and Co_3O_4 were combined with H_2O molecular to form Co − OH group on the surface of catalyst. (2) Co − OH complexes would connect with HSO_5^- though hydrogen bond. (3) The electrons discharged from Co^{2+} species break O—O bond of HSO_5^- through this connection, resulting in the generation of $SO_4^{\bullet-}$, then some $SO_4^{\bullet-}$ could react with water molecular or OH^- to generate •OH. (4) Co^{3+} could accept the electron from HSO_5^-, resulting in the cycle of Co^{2+}/Co^{3+} pairs. These steps can be described as Eq. (3)-Eq. (6) (Xie et al., 2018b; Yang et al., 2018b).

$$Co(II)+H_2O \rightarrow Co(II)\text{-}OH^+ + H^+ \quad (3)$$

$$Co(II)\text{-}OH^+ + HSO_5^- \rightarrow Co(III) - O^+ + SO_4^{\bullet-} + H_2O \quad (4)$$

$$SO_4^{\bullet-} + OH^-/H_2O \rightarrow {}^{\bullet}OH + H_2O \quad (5)$$

$$Co(III) - O^+ + H^+ + HSO_5^- \rightarrow Co(II) + SO_5^{\bullet-} + H_2O \quad (6)$$

$$2SO_5^{\bullet-} \rightarrow 2SO_4^{2-} + {}^1O_2 \quad (7)$$

$$HSO_5^- + Nu \rightarrow NuOH^+ + SO_4^{2-} \quad (8)$$

$$HSO_5^- + NuOH^+ \rightarrow SO_4^{2-}/HSO_4^- + {}^1O_2 + Nu + H^+ \quad (9)$$

The second one was the non-radical mechanism. $SO_5^{\bullet-}$ radicals could produce singlet oxygen during the process via the reaction described as Eq. (7) (Zou et al., 2019). Interestingly, a certain degree of RhB degradation could be observed in HAP/PMS system. As can be seen in Fig. 3b, pure PMS and HAP/PMS showed 0.4% and 33.4% of RhB removal, respectively. As described in previous literature, PMS can be decomposed to generate singlet oxygen with the assistant of nucleophile (Nu) tetrahedral PO_4 on HAP (Eq. (8)-Eq. (9)) (Song et al., 2018).

The generated singlet oxygen could react with RhB, resulting in the decomposition of this organic dye. The possible mechanism of PMS activation via Co-HAP catalyst was displayed in Fig. 4e.

3.3.2. Possible degradation pathway

To get a further insight into the degradation mechanism of RhB, UPLC-MS-MS analysis was employed to identify the intermediates produced during the reaction. TIC spectrum is shown in Fig. S1. The mass spectra, chemical structural formula and molecular weight of these intermediates are shown in Fig. S2. As can be seen, after treating in Co-HAP-2/PMS system, RhB degraded into six possible products. Based on previous studies and the results obtained in this work (Devi et al., 2019; Rachna Rani and Shanker, 2018; Rakibuddin et al., 2015; Sun et al., 2019b), the degradation pathway of RhB included four main processes: N-de-ethylation, Chromophore structure cleavage, Ring-opening and Mineralization, which is similar with other PMS/PS-based processes (Diao et al., 2017; Zeng et al., 2018). Firstly, the methyl groups dropped from RhB molecular via active species ($SO_4^{\bullet-}$, •OH and $^1O_2$) attack, leading to the generation of De-ethylation product. Secondly, the bond between xanthene group and phenyl group which is chromophore structure could be broken as the organics further degraded (*m/z* 318 and 274), resulting in the decolorization of RhB. Thirdly, low molecular weight acids (*m/z* 83, 94, 102 and 167) were generated from ring-opening process and further mineralized. The possible pathway of RhB degradation is illustrated in Fig. 6.

3.4. Co-catalytic effect of HAP on PMS activation

In this work, a phenomenon of great interest is that cobalt species showed remarkable enhancement of activity after combining with HAP, which is speculated to be the co-catalytic activity of Co-HAP. As being mentioned above, the formation of active sites $Co\text{-}OH^+$ is an important step in PMS activation by Co-based catalyst. In heterogeneous reaction, $Co\text{-}OH^+$ complexes would participate in PMS activation as described in Eq. (3)–(7). Based on above discussions, it could be speculated that higher amount of $Co\text{-}OH^+$ complexes could lead to better PMS activating performance of catalyst. Some researchers also found that the surface oxygen species might affect the amount of $Co\text{-}OH^+$ on catalyst surface during the reaction (Chen et al., 2018; Zhang et al., 2018). Therefore, XPS was employed to analyze oxygen species on fresh and used catalysts. As shown in Fig. 5c, two major peaks observed in O 1S spectra of Co_3O_4, which located at 531.1 eV and 529.7 eV, were assigned to lattice oxygen species (O_{lat}) (Hu et al., 2019) and surface oxygen species (O_{sur}) (Shi et al., 2014), respectively. The relative content of absorbed oxygen in Co_3O_4 phase revealed no change after the reaction, by contrast, the increase of relative content of absorbed oxygen can be observed in Co-HAP-2. In Fig. 5d, the peak located at 531.8 eV could be assigned to the O in PO_4^{3-} and OH groups (Fan et al., 2014), suggesting that more OH groups might form on Co-HAP-2 during the reaction. According to previous reports (Chong et al., 2018), HAP can provide both Lewis basics (O^{2-} in $-PO_4^{3-}$ - groups) and acidic sites (Ca^{2+} or OH- vacancies) on its surface. The Lewis acidic sites favor the adsorption/dissociation of water molecular, leading to the formation of surface $-OH$ group. Consequently, more $Co-OH^+$ were generated on the surface of Co-HAP-2, leading to higher radical yields. Besides, HAP could provide tetrahedral PO_4 to favor PMS decomposition, resulting in the generation of singlet oxygen. These two reasons can explain the possible mechanism for co-catalytic effect of HAP in Co-HAP/PMS system.

3.5. Stability and reusability of Co-HAP

The stability of Co-HAP-2 in sulfate radical-based oxidation process is also investigated. In recycle experiments, the used catalyst was centrifuged for 15 min and washed by pure water for the next run. Although the Co-HAP-2 samples without calcination showed a similar RhB degradation efficiency with the calcinated Co-HAP-2 samples (data not shown), the cobalt leaching of Co-HAP-2 without calcination was 1.30 mg/L, which was higher than the emission standard (1 mg/L, GB 25467-2010). As shown in Fig. 7, in the first run, the degradation efficiency was 93.6% after 12 min reaction, 0.71 mg/L of cobalt ion was leached into the solutions, which was lower than the emission standard, indicating that calcination was beneficial to the stability of Co-HAP-2. The degradation efficiency was 75.1% in the fourth run and the leaching concentrations of cobalt ion decreased slightly to 0.38 mg/L. Almost 20% reduction of degradation efficiency occurred in the fourth run, suggesting that the catalyst might be not suitable for more than 4 runs.

4. Conclusion

Co-HAP was synthesized successfully via an ion-exchanged method combined with calcination. The results of characterization indicated that Co species existed on Co-HAP in two forms: Co in lattice structure and Co_3O_4 on HAP surface. Novel Co-HAP catalyst was utilized to activate peroxymonosulfate for the degradation of organic contaminants. 93.3% of RhB could be degraded with 12 min. Co-HAP-2 exhibited superior catalytic activity which even better than that of $CoFe_2O_4$. Beside RhB, Co-HAP/PMS also displayed impressive performance in degradation various organic pollutants (AO7, TCH, LFX). The results of EPR and quenching experiments suggested that both radical and non-radical mechanism were involved in Co-HAP-2/PMS system and $^1O_2$ played a leading role in RhB degradation. The co-catalytic effect of HAP on PMS activation was due to that HAP favored the generation of Co-OH complexes leading to high yield of $SO_4^{\bullet-}$. The Co-HAP-2 catalyst was stable and reusable during first four runs. The present work may benefit the further improvement of Co-based catalysts for sulfate radical-based oxidation process.

The authors declare the following financial interests/personal relationships which may be considered as potential competing interests:

Declaration of Competing Interest

The authors declare that they have no known competing financial interests or personal relationships that could have appeared to influence the work reported in this paper.

Acknowledgements

This work was supported by the National Natural Science Foundation of China (U1501231, 21976042), The Project of Guangdong Provincial Key Laboratory of radioactive contamination control and resources (2017B030314182), Guangdong Key Laboratory of Environmental Catalysis and Health Risk Control (2018B030322014), the Science and Technology Research Programs of Guangzhou City (201804020072), the Hongkong Scholarship (XJ2016037), University's 2017 training program for young top-notch personnels (BJ201706). Guangdong Province Universities and Colleges Pearl River Scholar Funded Scheme (2018).

Appendix A. Supplementary data

Supplementary material related to this article can be found, in the online version, at doi:https://doi.org/10.1016/j.jhazmat.2019.121447.

References

Abdul Nasir Khan, M., Kwame Klu, P., Wang, C., Zhang, W., Luo, R., Zhang, M., Qi, J., Sun, X., Wang, L., Li, J., 2019. Metal-organic framework-derived hollow Co_3O_4/carbon as efficient catalyst for peroxymonosulfate activation. Chem. Eng. J. 363, 234–246.

Chen, L., Yang, S., Zuo, X., Huang, Y., Cai, T., Ding, D., 2018. Biochar modification significantly promotes the activity of Co_3O_4 towards heterogeneous activation of

peroxymonosulfate. Chem. Eng. J. 354, 856–865.
Chong, R., Fan, Y., Du, Y., Liu, L., Chang, Z., Li, D., 2018. Hydroxyapatite decorated TiO_2 as efficient photocatalyst for selective reduction of CO_2 with H_2O into CH_4. Int. J. Hydrogen Energy.
Cong, J., Lei, F., Zhao, T., Liu, H., Wang, J., Lu, M., Li, Y., Xu, H., Gao, J., 2017. Two Co-zeolite imidazolate frameworks with different topologies for degradation of organic dyes via peroxymonosulfate activation. J. Solid State Chem. 256, 10–13.
Deng, J., Ge, Y., Tan, C., Wang, H., Li, Q., Zhou, S., Zhang, K., 2017. Degradation of ciprofloxacin using α-MnO_2 activated peroxymonosulfate process: Effect of water constituents, degradation intermediates and toxicity evaluation. Chem. Eng. J. 330, 1390–1400.
Devi, M.M., Sunaina Singh, H., Kaur, K., Gupta, A., das, A., Nishanthi, S.T., Bera, C., Ganguli, A.K., Jha, M., 2019. New approach for the transformation of metallic waste into nanostructured Fe_3O_4 and SnO_2-Fe_3O_4 heterostructure and their application in treatment of organic pollutant. Waste Manage. 87, 719–730.
Diao, Z.-H., Liu, J.-J., Hu, Y.-X., Kong, L.-J., Jiang, D., Xu, X.-R., 2017. Comparative study of Rhodamine B degradation by the systems pyrite/H_2O_2 and pyrite/persulfate: reactivity, stability, products and mechanism. Sep. Purif. Technol. 184, 374–383.
Ding, C., Xiao, S., Lin, Y., Yu, P., Zhong, M.-e., Yang, L., Wang, H., Su, L., Liao, C., Zhou, Y., Deng, Y., Gong, D., 2019a. Attapulgite-supported nano-Fe^0/peroxymonsulfate for quinclorac removal: Performance, mechanism and degradation pathway. Chem. Eng. J. 360, 104–114.
Ding, M., Chen, W., Xu, H., Shen, Z., Lin, T., Hu, K., Kong, Q., Yang, G., Xie, Z., 2019b. Heterogeneous $Fe_2CoTi_3O_{10}$-MXene composite catalysts: Synergistic effect of the ternary transition metals in the degradation of 2,4-dichlorophenoxyacetic acid based on peroxymonosulfate activation. Chem. Eng. J. 378, 122177.
Ding, Y., Nie, W., Li, W., Chang, Q., 2019c. Co-doped $NaBiO_3$nanosheets with surface confined Co species: high catalytic activation of peroxymonosulfate and ultra-low Co leaching. Chem. Eng. J. 356, 359–370.
Fan, Z., Wang, J., Wang, Z., Ran, H., Li, Y., Niu, L., Gong, P., Liu, B., Yang, S., 2014. One-pot synthesis of graphene/hydroxyapatite nanorod composite for tissue engineering. Carbon 66, 407–416.
Fu, H., Ma, S., Zhao, P., Xu, S., Zhan, S., 2019. Activation of peroxymonosulfate by graphitized hierarchical porous biochar and $MnFe_2O_4$ magnetic nanoarchitecture for organic pollutants degradation: structure dependence and mechanism. Chem. Eng. J. 360, 157–170.
Guan, Y.-H., Ma, J., Liu, D.-K., Ou, Z.-f., Zhang, W., Gong, X.-L., Fu, Q., Crittenden, J.C., 2018. Insight into chloride effect on the UV/peroxymonosulfate process. Chem. Eng. J. 352, 477–489.
Guan, Y.H., Ma, J., Ren, Y.M., Liu, Y.L., Xiao, J.Y., Lin, L.Q., Zhang, C., 2013. Efficient degradation of atrazine by magnetic porous copper ferrite catalyzed peroxymonosulfate oxidation via the formation of hydroxyl and sulfate radicals. Water Res. 47, 5431–5438.
Han, M., Kong, L., Hu, X., Chen, D., Xiong, X., Zhang, H., Su, M., Diao, Z., Yang, R., 2018. Phase migration and transformation of uranium in mineralized immobilization by wasted bio-hydroxyapatite. J. Clean. Prod. 197, 886–894.
Hao, L., Lv, Y., Song, H., 2017. The morphological evolution of hydroxyapatite on high-efficiency Pb^{2+} removal and antibacterial activity. Microchem. J. 135, 16–25.
Hong, Y., Peng, J., Zhao, X., Yan, Y., Lai, B., Yao, G., 2019. Efficient degradation of atrazine by CoMgAl layered double oxides catalyzed peroxymonosulfate: optimization, degradation pathways and mechanism. Chem. Eng. J. 370, 354–363.
Hu, L., Deng, G., Lu, W., Pang, S., Hu, X., 2017. Deposition of CdS nanoparticles on MIL-53(Fe) metal-organic framework with enhanced photocatalytic degradation of RhB under visible light irradiation. Appl. Surf. Sci. 410, 401–413.
Hu, L., Zhang, G., Liu, M., Wang, Q., Wang, P., 2018a. Enhanced degradation of bisphenol A (BPA) by peroxymonosulfate with Co_3O_4-Bi_2O_3 catalyst activation: effects of pH, inorganic anions, and water matrix. Chem. Eng. J. 338, 300–310.
Hu, M., Yao, Z., Liu, X., Ma, L., He, Z., Wang, X., 2018b. Enhancement mechanism of hydroxyapatite for photocatalytic degradation of gaseous formaldehyde over TiO_2/hydroxyapatite. J. Taiwan Inst. Chem. E 85, 91–97.
Hu, P., Long, M., 2016. Cobalt-catalyzed sulfate radical-based advanced oxidation: a review on heterogeneous catalysts and applications. Appl. Catal. B: Environ. 181, 103–117.
Hu, T., Wang, Y., Zhang, L., Tang, T., Xiao, H., Chen, W., Zhao, M., Jia, J., Zhu, H., 2019. Facile synthesis of PdO-doped Co_3O_4 nanoparticles as an efficient bifunctional oxygen electrocatalyst. Appl. Catal. B: Environ. 243, 175–182.
Huang, G.-X., Wang, C.-Y., Yang, C.-W., Guo, P.-C., Yu, H.-Q., 2017. Degradation of Bisphenol A by peroxymonosulfate catalytically activated with $Mn_{1.8}Fe_{1.2}O_4$ nanospheres: synergism between Mn and Fe. Environ. Sci. Technol. 51, 12611–12618.
Jung, K.-W., Lee, S.Y., Choi, J.-W., Lee, Y.J., 2019. A facile one-pot hydrothermal synthesis of hydroxyapatite/biochar nanocomposites: Adsorption behavior and mechanisms for the removal of copper(II) from aqueous media. Chem. Eng. J. 369, 529–541.
Li, C., Wu, J., Peng, W., Fang, Z., Liu, J., 2019a. Peroxymonosulfate activation for efficient sulfamethoxazole degradation by Fe_3O_4/β-FeOOH nanocomposites: coexistence of radical and non-radical reactions. Chem. Eng. J. 356, 904–914.
Li, Z., Ma, S., Xu, S., Fu, H., Li, Y., Zhao, P., Meng, Q., 2019b. Heterogeneous catalytic degradation of organic pollutants by peroxymonosulfate activated with nitrogen doped graphene oxide loaded $CuFe_2O_4$. Colloids Surf. A Physicochem. Eng. Asp. 577, 202–212.
Lin, H., Li, S., Deng, B., Tan, W., Li, R., Xu, Y., Zhang, H., 2019. Degradation of bisphenol A by activating peroxymonosulfate with $Mn_{0.6}Zn_{0.4}Fe_2O_4$ fabricated from spent Zn-Mn alkaline batteries. Chem. Eng. J. 364, 541–551.
Lin, K.-Y.A., Yang, M.-T., Lin, J.-T., Du, Y., 2018. Cobalt ferrite nanoparticles supported on electrospun carbon fiber as a magnetic heterogeneous catalyst for activating peroxymonosulfate. Chemosphere 208, 502–511.
Ling, S.K., Wang, S., Peng, Y., 2010. Oxidative degradation of dyes in water using Co^{2+}/H_2O_2 and Co^{2+}/peroxymonosulfate. J. Hazard. Mater. 178, 385–389.
Liu, J., Zhao, Z., Shao, P., Cui, F., 2015. Activation of peroxymonosulfate with magnetic Fe_3O_4–MnO_2 core–shell nanocomposites for 4-chlorophenol degradation. Chem. Eng. J. 262, 854–861.
Liu, X., Ma, J., Yang, J., 2014. Visible-light-driven amorphous Fe(III)-substituted hydroxyapatite photocatalyst: characterization and photocatalytic activity. Mater. Lett. 137, 256–259.
Liu, Y., Guo, H., Zhang, Y., Cheng, X., Zhou, P., Deng, J., Wang, J., Li, W., 2019. Highly efficient removal of trimethoprim based on peroxymonosulfate activation by carbonized resin with Co doping: performance, mechanism and degradation pathway. Chem. Eng. J. 356, 717–726.
Pi, Y., Gao, H., Cao, Y., Cao, R., Wang, Y., Sun, J., 2020. Cobalt ferrite supported on carbon nitride matrix prepared using waste battery materials as a peroxymonosulfate activator for the degradation of levofloxacin hydrochloride. Chem. Eng. J. 379, 122377.
Qi, C., Liu, X., Lin, C., Zhang, H., Li, X., Ma, J., 2017. Activation of peroxymonosulfate by microwave irradiation for degradation of organic contaminants. Chem. Eng. J. 315, 201–209.
Rachna Rani, M., Shanker, U., 2018. Enhanced photocatalytic degradation of chrysene by Fe_2O_3@ZnHCF nanocubes. Chem. Eng. J. 348, 754–764.
Rakibuddin, M., Gazi, S., Ananthakrishnan, R., 2015. Iron(II) phenanthroline-resin hybrid as a visible light-driven heterogeneous catalyst for green oxidative degradation of organic dye. Catal. Commun. 58, 53–58.
Shao, P., Duan, X., Xu, J., Tian, J., Shi, W., Gao, S., Xu, M., Cui, F., Wang, S., 2017. Heterogeneous activation of peroxymonosulfate by amorphous boron for degradation of bisphenol S. J. Hazard. Mater. 322, 532–539.
Shen, Y., Wang, L., Wu, Y., Li, X., Zhao, Q., Hou, Y., Teng, W., 2015. Facile solvothermal synthesis of $MnFe_2O_4$ hollow nanospheres and their photocatalytic degradation of benzene investigated by in situ FTIR. Catal. Commun. 68, 11–14.
Shi, P., Dai, X., Zheng, H., Li, D., Yao, W., Hu, C., 2014. Synergistic catalysis of Co_3O_4 and graphene oxide on Co_3O_4/GO catalysts for degradation of Orange II in water by advanced oxidation technology based on sulfate radicals. Chem. Eng. J. 240, 264–270.
Šljivić Ivanović, M., Smičiklas, I., Pejanović, S., 2013. Analysis and comparison of mass transfer phenomena related to Cu^{2+} sorption by hydroxyapatite and zeolite. Chem. Eng. J. 223, 833–843.
Song, F., Zhang, H., Wang, S., Liu, L., Tan, X., Liu, S., 2018. Atomic-level design of $CoOH^+$–hydroxyapatite@C catalysts for superfast degradation of organics via peroxymonosulfate activation. Chem. Commun. 54, 4919–4922.
Sun, H., Peng, X., Zhang, S., Liu, S., Xiong, Y., Tian, S., Fang, J., 2017. Activation of peroxymonosulfate by nitrogen-functionalized sludge carbon for efficient degradation of organic pollutants in water. Bioresour. Technol. Rep. 241, 244–251.
Sun, P., Liu, H., Feng, M., Guo, L., Zhai, Z., Fang, Y., Zhang, X., Sharma, V.K., 2019a. Nitrogen-sulfur co-doped industrial graphene as an efficient peroxymonosulfate activator: singlet oxygen-dominated catalytic degradation of organic contaminants. Appl. Catal. B: Environ. 251, 335–345.
Sun, X., Yan, L., Xu, R., Xu, M., Zhu, Y., 2019b. Surface modification of TiO_2 with polydopamine and its effect on photocatalytic degradation mechanism. Colloids Surf. A Physicochem. Eng. Asp. 570, 199–209.
Tan, C., Gao, N., Deng, Y., Deng, J., Zhou, S., Li, J., Xin, X., 2014. Radical induced degradation of acetaminophen with Fe_3O_4 magnetic nanoparticles as heterogeneous activator of peroxymonosulfate. J. Hazard. Mater. 276, 452–460.
Tu, Y., Tian, S., Kong, L., Xiong, Y., 2012. Co-catalytic effect of sewage sludge-derived char as the support of Fenton-like catalyst. Chem. Eng. J. 185-186, 44–51.
Valizadeh, S., Rasoulifard, M.H., Dorraji, M.S.S., 2014. Modified Fe_3O_4-hydroxyapatite nanocomposites as heterogeneous catalysts in three UV, Vis and Fenton like degradation systems. Appl. Surf. Sci. 319, 358–366.
Wang, G., Cheng, C., Zhu, J., Wang, L., Gao, S., Xia, X., 2019a. Enhanced degradation of atrazine by nanoscale LaFe1-xCuxO_3-delta perovskite activated peroxymonosulfate: Performance and mechanism. Sci. Total Environ. 673, 565–575.
Wang, N., Lv, H., Zhou, Y., Zhu, L., Hu, Y., Majima, T., Tang, H., 2019b. Complete defluorination and mineralization of perfluorooctanoic acid by a mechanochemical method using alumina and persulfate. Environ. Sci. Technol. 53, 8302–8313.
Wang, X., Tang, P., Ding, C., Cao, X., Yuan, S., Zuo, X., Deng, X., 2017. Simultaneous enhancement of adsorption and peroxymonosulfate activation of Nitrogen-doped reduced graphene oxide for bisphenol A removal. J. Environ. Chem. Eng. 5, 4291–4297.
Wang, Y.-Y., Liu, Y.-X., Lu, H.-H., Yang, R.-Q., Yang, S.-M., 2018. Competitive adsorption of Pb(II), Cu(II), and Zn(II) ions onto hydroxyapatite-biochar nanocomposite in aqueous solutions. J. Solid State Chem. 261, 53–61.
Xie, J., Wei, Y., Song, X., Chen, Y., Zou, Q., Wang, M., Xu, A., Li, X., 2018a. Controlled growth of γ-MnO_2 nanoflakes on OMS-2 for efficient decomposition of organic dyes in aqueous solution via peroxymonosulfate activation. J. Colloid Interface Sci. 529, 476–485.
Xie, R., Ji, J., Huang, H., Lei, D., Fang, R., Shu, Y., Zhan, Y., Guo, K., Leung, D.Y.C., 2018b. Heterogeneous activation of peroxymonosulfate over monodispersed Co_3O_4/activated carbon for efficient degradation of gaseous toluene. Chem. Eng. J. 341, 383–391.
Yang, Q., Yang, X., Yan, Y., Sun, C., Wu, H., He, J., Wang, D., 2018a. Heterogeneous activation of peroxymonosulfate by different ferromanganese oxides for tetracycline degradation: Structure dependence and catalytic mechanism. Chem. Eng. J. 348, 263–270.
Yang, S., Qiu, X., Jin, P., Dzakpasu, M., Wang, X.C., Zhang, Q., zhang, L., Yang, L., Ding, D., Wang, W., Wu, K., 2018b. MOF-templated synthesis of $CoFe_2O_4$ nanocrystals and its coupling with peroxymonosulfate for degradation of bisphenol A. Chem. Eng. J.

353, 329–339.
Yang, S., Wu, P., Liu, J., Chen, M., Ahmed, Z., Zhu, N., 2018c. Efficient removal of bisphenol A by superoxide radical and singlet oxygen generated from peroxymonosulfate activated with Fe^0-montmorillonite. Chem. Eng. J. 350.
Ye, T., Wei, Z., Spinney, R., Tang, C.-J., Luo, S., Xiao, R., Dionysiou, D.D., 2017. Chemical structure-based predictive model for the oxidation of trace organic contaminants by sulfate radical. Water Res. 116, 106–115.
Yin, R., Guo, W., Wang, H., Du, J., Zhou, X., Wu, Q., Zheng, H., Chang, J., Ren, N., 2018. Enhanced peroxymonosulfate activation for sulfamethazine degradation by ultrasound irradiation: Performances and mechanisms. Chem. Eng. J. 335, 145–153.
Yuan, R., Hu, L., Yu, P., Wang, H., Wang, Z., Fang, J., 2018. Nanostructured Co_3O_4grown on nickel foam: An efficient and readily recyclable 3D catalyst for heterogeneous peroxymonosulfate activation. Chemosphere 198, 204–215.
Zeng, H., Zhang, W., Deng, L., Luo, J., Zhou, S., Liu, X., Pei, Y., Shi, Z., Crittenden, J., 2018. Degradation of dyes by peroxymonosulfate activated by ternary CoFeNi-layered double hydroxide: catalytic performance, mechanism and kinetic modeling. J Colloid Interface Sci. 515, 92–100.
Zhang, A.-Y., He, Y.-Y., Chen, Y.-P., Feng, J.-W., Huang, N.-H., Lian, F., 2018. Degradation of organic pollutants by Co_3O_4-mediated peroxymonosulfate oxidation: roles of high-energy {0 0 1}-exposed TiO_2 support. Chem. Eng. J. 334, 1430–1439.
Zhang, L., Yang, X., Han, E., Zhao, L., Lian, J., 2017. Reduced graphene oxide wrapped Fe_3O_4–Co_3O_4 yolk–shell nanostructures for advanced catalytic oxidation based on sulfate radicals. Appl. Surf. Sci. 396, 945–954.
Zhang, Q., Jing, Y.H., Shiue, A., Chang, C.-T., Chen, B.-Y., Hsueh, C.-C., 2012. Deciphering effects of chemical structure on azo dye decolorization/degradation characteristics: bacterial vs. photocatalytic method. J. Taiwan Inst. Chem. E 43, 760–766.
Zhu, C., Liu, F., Ling, C., Jiang, H., Wu, H., Li, A., 2019. Growth of graphene-supported hollow cobalt sulfide nanocrystals via MOF-templated ligand exchange as surface-bound radical sinks for highly efficient bisphenol A degradation. Appl. Catal. B: Environ. 242, 238–248.
Zou, Y., Li, W., Yang, L., Xiao, F., An, G., Wang, Y., Wang, D., 2019. Activation of peroxymonosulfate by sp2-hybridized microalgae-derived carbon for ciprofloxacin degradation: importance of pyrolysis temperature. Chem. Eng. J. 370, 1286–1297.